Ceramics International 44 (2018) 3893–3903

Contents lists available at ScienceDirect

Ceramics International

journal homepage: www.elsevier.com/locate/ceramint

Porous cordierite-based ceramics processed by starch consolidation casting – Microstructure and high-temperature mechanical behavior

M. Laura Sandoval[a,*], Mariano H. Talou[a], Analía G. Tomba Martinez[a], M. Andrea Camerucci[a], Eva Gregorová[b], Willi Pabst[b]

[a] Ceramics Division, Research Institute for Materials Science and Technology (INTEMA), CONICET/UNMdP, Mar del Plata, Buenos Aires B7608FDQ, Argentina
[b] Department of Glass and Ceramics, University of Chemistry and Technology, Prague (UCT Prague), 166 28 Prague 6, Czech Republic

ARTICLE INFO

Keywords:
Cordierite
Porosity
Microstructure-final
Mechanical properties

ABSTRACT

Porous cordierite-based ceramics with different microstructural features and mechanical behavior were formed by starch consolidation casting (SCC) using native potato and corn starches and sintered at 1275, 1300 and 1330 °C. The composition and microstructure of the ceramic materials were investigated via quantitative phase analysis using X-ray diffraction (with Rietveld refinement), the Archimedes method, mercury porosimetry, scanning electron microscopy and optical microscopy with stereology-based image analysis. The mechanical behavior of samples was evaluated by diametral compression tests at room temperature, 1000 and 1100 °C. The type of starch used and the sintering temperatures were the main factors determining the characteristics of the developed porous microstructures. Materials prepared with corn starch achieved the lowest porosity and the lowest values of mean chord length, mean pore distance and pore throat size. Because of these features, these materials thus presented, in general, higher values of apparent Young's modulus, elastic limit and mechanical strength than those prepared with potato starch. Despite the presence of a silicate glassy phase, both porous materials, mainly those prepared with corn starch, still enhanced the basic mechanical properties at high temperature, in particular, the mechanical strength and the apparent Young's modulus due to the special combination of the porous microstructure features.

1. Introduction

Cordierite ceramics ($Mg_2Al_4Si_5O_{18}$) are well known for their low thermal expansion coefficient, which provides them with a high thermal shock resistance suitable for applications involving temperature cycling. Therefore, in combination with satisfactory mechanical properties, chemical stability and corrosion resistance, low thermal conductivity, a low dielectric constant and low dielectric loss factor, the range of applications for cordierite-based ceramics is very wide, ranging from kiln furniture [1] and thermally and electrically insulating ceramics [2,3] to diesel particulate filters [4] and other filters [5], as well as membrane supports [6], catalyst supports [7] and electronic substrates [8], to name only the most important. Although the properties of cordierite-based ceramics have been investigated for quite some time [9–11], a look into the current literature shows that their processing and properties are still among the hot topics of ceramic research and development [12–14].

Nowadays, porous cordierite-based ceramics and ceramic foams in which the thermal insulation behavior, specific surface and permeability can be tailored by controlling the porosity, pore surface area and pore size (and shape), are of particular interest [15–21]. In this field, one of the early applications of starch consolidation casting (SCC) concerned cordierite ceramics [15,17,18].

Currently, the problem is that cordierite-based ceramics, especially those types that are prepared by cheap natural raw materials (mainly kaolin and talc), are complex multiphase materials that may contain, apart from cordierite as the main phase, several other crystalline phases (mullite, alumina, cristobalite, magnesia-alumina spinel [13,14,22,23], enstatite [14,24] and sapphirine [24]) and usually a siliceous glassy phase [23]. When natural raw materials are used, it is clear that even for nominally similar compositions the resulting materials can be different and exhibit different properties. This has significant implications for industrial production, because the raw materials that are available in a certain region of the world may differ from those available elsewhere.

Previous work by the authors concerned porous cordierite-based ceramics prepared by SCC from Argentinian kaolin and Chinese talc, and using potato and cassava (tapioca) starches as a pore former and

* Corresponding author's.
E-mail address: laura.sandoval@fi.mdp.edu.ar (M.L. Sandoval).

https://doi.org/10.1016/j.ceramint.2017.11.180
Received 19 September 2017; Received in revised form 7 November 2017; Accepted 24 November 2017
Available online 01 December 2017

stiffener [17,18]. While talc is a strategic raw material for which world production is largely concentrated in certain countries (mainly China, Australia and USA) [25] and distributed by a few world-wide companies, kaolin is usually from more local deposits that differ from region to region. In Central Europe, for example, Czech kaolin is one of the most widely used. On the other hand, cassava (tapioca) starch is not commonly produced in many industrialized regions of the world, such as in Europe. Therefore, the present work investigates the porous microstructures developed in cordierite-based ceramics prepared from Czech kaolin, Australian talc and potato and corn starches. Moreover, the high temperature mechanical behavior of cordierite-based ceramics, an aspect that has been scarcely studied in spite of its importance for successful applications of these materials, was also investigated. Finally, the obtained results were discussed from the viewpoint of phase evolution, microstructure and high-temperature mechanical properties.

2. Experimental procedure

2.1. Processing and characterization of porous green bodies

A cordierite precursor mixture (denoted PM) composed of kaolin 37 wt% (Sedlec Ia, Sedlecký kaolin a.s., Božičany, Czech Republic), talc 41 wt% (EC 75, Luzenac Group, Three Springs, Australia) and alumina 22 wt% (CT3000 SG, Almatis GmbH, Ludwigshafen, Germany) was used as raw ceramic material for obtaining cordierite-based bodies [26]. Commercially available potato starch (Solamyl, Natura a.s., Havlíčkův Brod, Czech Republic) and corn starch (Gustin, Dr. Oetker, Kladno, Czech Republic) were used as stiffening agents (binders) and pore formers. The complete characterization of both the ceramic and starch powders was reported in a previous work by the authors [26]. The main features of the raw materials used are shown in Table 1.

Green disks 18.6 ± 0.9 mm in diameter and 3.7 ± 0.7 mm in height were formed by SCC. Aqueous ceramic-starch (PM-potato or PM-corn) suspensions with a total solid content of 60 wt% were prepared by mixing (impeller mixer) ceramic powders in distilled water with 1 wt% Dolapix CE-64 (Zschimmer & Schwarz, Lahnstein, Germany) and 0.5 wt % sodium napthalenesulfonate (Nutrimer Argentina S.A., Buenos Aires, Argentina), both amounts with respect to the ceramic solid content, homogenizing in a ball mill for 4 h, degassing for 20 min, and finally homogenizing the inorganic solids with starch and extra water for 1–2 min in order to obtain the desired total solid loading. The experimental conditions used for preparing these systems were previously established and reported [26]. The volume fraction of starch related to the suspension volume (15 vol%) was calculated by considering the pycnometric density value (2.40 ± 0.05 g/cm^3) determined by He-pycnometry for the precursor mixture with starch. This amount was selected taking into account previously obtained results [27] and data reported in the literature in order to obtain ceramic materials with porosities higher than 35% by starch consolidation casting [28].

The prepared suspensions were poured into cylindrical stainless steel molds which were covered with Teflon, and subsequently heated in an electric stove with forced circulation of air (UFP 400, Memmert, Schwabach, Germany) at 80 °C for 4 h and dried at 40 °C for 12 h. The experimental conditions (temperature and dwell time) used for the consolidation of suspensions were established on the basis of results previously reported by the authors [17] and other published data [15]. Once the consolidation was completed, the samples were taken out of their molds.

A previous study [26] indicated that the total green porosity of the both materials was very similar (38 ± 6% for PM-potato and 36 ± 5% for PM-corn) and only a small amount of cavities with starch-granule-specific morphology and interconnected channels (windows) in the cavity walls were developed. These particular features, which were not usually reported in previous work [29,30], could be attributed to the combined effect of certain specific characteristics of the gelatinization process and the presence of phyllosilicate raw materials with oblate particles (kaolin and talc) in the studied systems [26].

2.2. Microstructural evolution as a function of temperature

Thermal treatments for the calcining and reaction-sintering of green disks were performed in an electric furnace with SiC heating elements (RHF 16/3, Carbolite, Hope Valley, UK). Three sintering temperatures (T_s) were applied, viz., 1275, 1300 and 1330 °C, while keeping the thermal cycle constant as follows: heating rate 1 °C/min up to 650 °C; 2 h dwell at 650 °C; heating rate 3 °C/min up to T_s, 4 h dwell at T_s; cooling rate 5 °C/min down to room temperature. The burnout temperature (650 °C) was selected based on previous results from thermogravimetric analyses (TGA-50, Shimadzu, Kyoto, Japan; at 10 °C/min up to 700 °C, in air) of the native starches. During the first stage of the thermal treatment (≤ 650 °C), complete removal of the starch and organic additives is achieved (burnout), together with the dehydroxylation of kaolinite, while dehydroxylation of talc and the reaction of the ceramic precursors occur, concomitantly with sintering, during the second stage (reaction-sintering).

The crystalline phase evolution as a function of T_s was studied by qualitative and semi-quantitative phase analysis via X-ray diffraction (X'Pert PRO, PANalytical, Almelo, The Netherlands, with Cu K_α radiation at 40 kV and 40 mA, and 0.01 steps per second) of powder samples of sintered disks. In particular, semi-quantitative analysis was performed using Rietveld refinement, which was carried out employing a commercial multipurpose profile-fitting software (FullProf) [31]. The general methodology employed to obtain the phase contents from the Rietveld optimized scale factors normalizes the results to 100% of crystalline phases (i.e. the presence of an amorphous phase is not taken into account). Nevertheless, bearing in mind that a siliceous liquid phase is generated during the thermal treatments of the cordierite precursor mixture used in this work, and therefore, a silicate glassy

Table 1
Characterization of raw materials.

Raw materials	Chemical analysis	Mineralogical analysis	D_{50} (μm)
Kaolin	Al_2O_3/SiO_2 = 0.8	Kaolinite[a] ($Al_2Si_2O_5(OH)_4$)	3.2
	Fe_2O_3, CaO, MgO, Na_2O < 1.9 wt%	Quartz[b] (SiO_2)	
	K_2O ~ 0.9 wt%	Halloysite[b] ($Al_2Si_2O_5(OH)_4$)	
Talc	SiO_2/MgO = 1.9		9.0
	Fe_2O_3 ~ 0.9 wt%	Talc[a] ($Mg_3Si_4O_{10}(OH)_2$)	
	CaO ~ 0.4 wt%	Traces of hematite (Fe_2O_3)	
Alumina	Al_2O_3 = 99.85 wt%	Corundum (Al_2O_3)	0.8
	Alkaline, alk. earth impurities < 0.2 wt%		
	Silica, iron oxides ~ 0.05 wt%		
Potato starch	Polysaccharide $(C_6H_{10}O_5)_n$, trace elements K, P, Ca < 0.2 wt%, in total		45
Corn starch	Polysaccharide $(C_6H_{10}O_5)_n$, trace elements K, P, Na, Cl < 0.2 wt% in total		15

[a] Majority phase.
[b] secondary phase.

phase is present in the sintered materials along with several crystalline phases, Ohlberg's method [32] was used for determining the content of the glass phase present in the final materials. In this case, the amorphous phase percentage is determined by interpolating the signal at 22.5°2θ of the diffractogram corresponding to the sample being studied with those obtained for an amorphous silica phase and a fully crystalline phase (silica or silicon). In this work, the diffractograms obtained for a sample of amorphous silica and for a commercial silicon powder (Sigma-Aldrich, Milwaukee, WI) were used in order to quantify the glass phase developed in the final materials by using the previously mentioned method.

Bulk densities (ρ) and open porosities ($\%P_{open}$) of disks sintered at different T_s were determined by the Archimedes method in water. The total porosity ($\%P_{total}$) of the sintered materials was calculated from $100\cdot(1-\rho/\rho_0)$, where ρ_0 is the true density of the material. This value after sintering at 1275 °C (ρ_0 = 2.87 g/cm^3), 1300 °C (ρ_0 = 2.81 g/cm^3) and 1330 °C (ρ_0 = 2.68 g/cm^3) was calculated from each phase composition obtained by XRD via Rietveld refinement (including the glass phase estimate) and the corresponding theoretical densities [24,33]. The closed porosity ($\%P_{closed}$) was calculated from the difference between $\%P_{total}$ and $\%P_{open}$.

First, the analysis of the microstructures developed as a function of temperature was performed by SEM (JSM-6460, JEOL, Tokyo, Japan) on the fracture surface of disks. Based on this analysis, the degree of sintering, homogeneity, grain size, grain morphology and presence of cell windows were evaluated.

In addition, global metric descriptors obtained via stereological relations (stereology being defined as the method to derive a quantitative description of 3D geometry from the quantitative analysis of 2D images) were determined by analyzing images captured by optical microscopy (PMG-3, Olympus, Tokyo, Japan) on planar surfaces in order to complete the microstructural analysis. Surfaces were mechanized by grinding with 600-grit SiC paper using water as a lubricant, and then polishing them with 3 μm and 1 μm diamond pastes on nylon cloth lubricated with a commercial solvent. Details concerning these calculations can be found in a recent paper [34]. The analysis of the corresponding images was carried out using image analysis software (Lucia G, Laboratory Imaging, Prague, Czech Republic). However, instead of processing and binarizing the images and applying automatic image analysis, which is often prone to introducing considerable bias, a manual procedure with software-based data acquisition was adopted: square grids were superimposed directly on the images of the planar sections to be analyzed and all quantities were determined by counting, not by measuring techniques. Depending on the pore size and image magnification, the square lattices used were 16 × 11 and 12 × 8, corresponding to 17 × 12 and 13 × 9 probe lines, respectively. The corresponding numbers of grid points were 204 and 117, respectively. Surface densities, mean chord lengths and mean distances were determined by counting the intersection points of lines with pore section outlines (161–317 intersection points), and mean curvature integral densities were determined by counting convex and concave tangent points (325–664 tangent points). Errors and 95% confidence intervals were calculated according to the formulas given in the aforementioned paper [34].

In addition, mercury porosimetry (AutoPore IV 9500, Micromeritics, Aachen, Germany) was used to determine the pore throat size distributions in the materials sintered at 1330 °C, 4 h.

2.3. Mechanical behavior

The mechanical behavior of the final materials sintered at 1330 °C (selected temperature based on the results obtained from the phase analysis and microstructural analysis) was assessed by diametral compression at room temperature, 1000 and 1100 °C, on a number of disks considered sufficient for statistical purposes. An INSTRON model 8501 servohydraulic machine (Instron Ltd, High Wycombe, Bucks, UK) with high stiffness was used for all tests. The tests at room temperature were carried out using steel plates (HRc 65), with a controlled displacement rate (of the actuator) of 0.2 mm/min. MoS_2 lubricant paste was used in order to reduce the effect of friction between the specimen and the platens.

In addition, the high temperature tests were performed using alumina/mullite rods with a diameter of 60 mm, with a controlled displacement rate (of the actuator) of 0.7 mm/min. Moreover, an electric furnace (heating elements of $MoSi_2$; Severn Furnace Ltd, Bristol, UK) was coupled to the machine, using a heating rate of 5 °C/min up to the test temperature (1000–1100 °C).

The diameter (D) of the tested disks was four times larger than the thickness (t) to ensure that only a plane stress state was tested in the analysis ($t/D \leq 0.25$) [35]. This assumption is implicit in the theoretical treatment of the diametral compression loading case (Eq. (1)) [35,36]. From experimental load vs. displacement curves, the apparent stress (σ)–strain (ε) relationship was calculated using the following equations:

$$\sigma = \frac{2F}{\pi D t} \quad (1)$$

$$\varepsilon = \frac{d}{D} \quad (2)$$

where F is the fracture load, D and t are the diameter and the thickness of the disk, respectively, and d is the actuator displacement [35–39].

From the σ vs. ε curves, the following parameters were determined: a) the mechanical strength (σ_F) using the maximum peak load, b) the fracture strain (ε_F) considered to be the deformation corresponding to the maximum stress, c) the apparent Young's modulus (E_a) as the slope of the linear part of the curves, and d) the elastic limit (σ_Y) defined as the stress where the curve deviates from linearity [37]. Moreover, the σ_Y/σ_F ratio expressed as a percentage was calculated and considered as the degree of deviation from the linear behavior caused by irreversible strain mechanisms (e.g. global plasticity and/or localized plasticity, and microcracking), i.e., the degree of plasticity. Indeed, the E_a parameter is the product of the Poisson's ratio and the Young's modulus of the material, and it is considered as an elastoplastic tangent modulus [26]. The crack patterns of tested disks were also analyzed.

3. Results and discussion

3.1. Analysis of the phase thermal evolution

The XRD patterns of materials, obtained after firing at the different temperatures (T_s) studied, are shown in Fig. 1. In this figure, only the main peaks of the majority crystalline phases are indicated. The

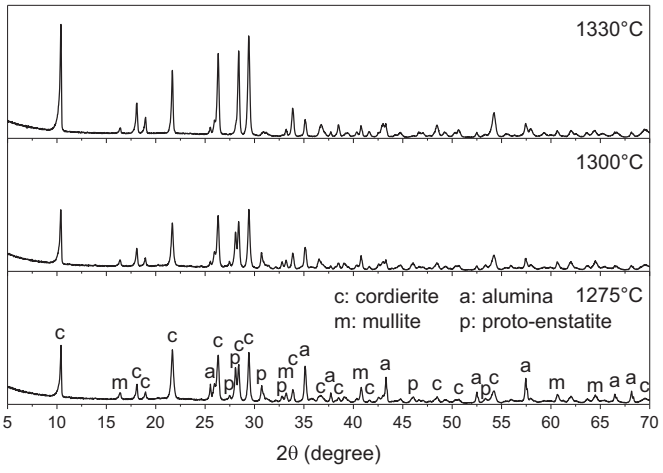

Fig. 1. XRD patterns of powdered samples treated at 1275, 1300 and 1330 °C, 4 h.

Table 2
Phase contents in samples treated at 1275, 1300 and 1330 °C, 4 h.

Phase	Content (wt%)		
	1275 °C	1300 °C	1330 °C
Cordierite	26.9	34.6	59.2
Mullite	19.3	18.4	14.6
Alumina	13.7	5.1	6.5
Proto-enstatite	12.9	15.4	1.2
Cristobalite	5.4	2.1	–
Sapphirine	2.7	5.6	–
Spinel	1.0	0.8	3.5
Glass phase	18.1	18.0	15.0

crystalline phase contents determined by Rietveld refinement for samples treated at 1275, 1300 and 1330 °C, together with the estimated silicate glassy phase contents, are shown in Table 2.

Based on the XRD pattern of the sample sintered at 1275 °C, cordierite ($2Al_2O_3.5SiO_2.2MgO$, JCPDS File 13-0294) and mullite ($3Al_2O_3.2SiO_2$, JCPDS File 79-1276) were determined as main crystalline phases (~ 27 and ~ 19 wt%, respectively), together with alumina in the form of corundum (α-Al_2O_3, JCPDS File 74-0323) and proto-enstatite (orthorhombic SiO_2. MgO, JCPDS File 76-1806) as secondary phases (~ 14 and ~ 13 wt%, respectively). In addition, diffraction peaks of very low intensity corresponding to cristobalite (SiO_2, JCPDS File 04-0379), sapphirine ($5Al_2O_3.2SiO_2.4MgO$, JCPDS File 76-0537) and spinel ($Al_2O_3.MgO$, JCPDS File 77-1193) phases (the content of these phases was < 6 wt%), together with a band located between 20–30 °2θ, assigned to the non-crystalline silicate phase (~ 18 wt%), were also identified. The origin of this last phase was associated with the impurities present in the raw materials and the liquid phase formed during the thermal treatment.

For the samples sintered at 1300 °C, diffraction peaks corresponding to cordierite, proto-enstatite and mullite were determined, together with diffraction peaks of low intensity of alumina, sapphirine, spinel and cristobalite. The diffraction peaks of the first two phases were of higher intensity than those present in samples treated at 1275 °C, while the intensities of peaks assigned to mullite remained unchanged. The amount of cordierite and proto-enstatite increased by ~ 8 and ~ 3 wt%, respectively (compared to the sample treated at 1275 °C), while the mullite content remained approximately the same (Table 2). The intensity of the band located between 20° and 30° 2θ was similar to that observed in the XRD pattern of the sample sintered at 1275 °C.

Finally, in the materials sintered at 1330 °C, cordierite diffraction peaks were much more intense and narrow than those for the materials treated at 1275 or 1300 °C, which can be associated with crystallite growth or an increase in the degree of crystallinity for this phase, while the diffraction peaks corresponding to mullite were of slightly lower intensity than those corresponding to the remaining XRD patterns. In addition, alumina and spinel were identified as secondary phases together with traces of proto-enstatite, while cristobalite and sapphirine phases were not determined in this case. The intensities of the diffraction peaks assigned to the proto-enstatite phase and the band corresponding to the glass phase were notably lower (~ 1 and ~ 15 wt% were determined for the crystalline and glass phases, respectively) than those registered in the diffractogram of the sample sintered at 1300 °C. The quantification of phase contents indicated that the phases present in the precursor mixture evolved by heating at 1330 °C to form a material based on cordierite (~ 60 wt%) and mullite (~ 15 wt%), with alumina (6.5 wt%) and spinel (3.5 wt%) as minor phases.

It is well known that one of the most important features of the $MgO.Al_2O_3$. SiO_2 ternary diagram is the existence of five eutectic points around the cordierite field with temperatures between 1345 and 1460 ± 5 °C. Because of this particularity, small variations in the chemical composition with regard to the stoichiometric cordierite composition can lead to the crystallization of minor phases together with cordierite as a main phase. Minor phases such as mullite, corundum, spinel, enstatite, forsterite, sapphirine can coexist with cordierite [40]. Moreover, it is known that in any process of cordierite synthesis, the phase composition is difficult to predict because it depends on the temperature, time and synthesis route. On the other hand, the crystallization of cordierite occurs by two mechanisms: the diffusion of Mg and Al cations into silicate liquid phases and the solid-state reaction between the magnesium-, aluminium- and silicon-containing phases. Both mechanisms require extremely restricted conditions that hinder the synthesis of single-phase cordierite ceramics.

Based on the quantitative results obtained (Table 2), and considering data reported in the literature for similar systems [41], it appears that in the present work, the formation of the cordierite phase occurs first due to a solid state reaction between mullite, proto-enstatite and amorphous silica. Mullite is primarily formed at ~ 1000 °C from the thermal decomposition of kaolinite (which begins with its dehydroxylation at temperatures around 600 °C) while proto-enstatite, which is the stable polymorph of enstatite at high temperature, is derived from the decomposition of talc. Amorphous silica is generated from the thermal decomposition of both kaolinite and talc. In addition to the primary mullite formed at temperatures around 1000 °C, mullite (so-called secondary mullite) could also have been generated during the thermal treatments at higher temperature, probably at 1300 °C, from a reaction between alumina and amorphous silica, which could explain the decrease in the amount of alumina and the constancy of the mullite content when the temperature increases from 1275 to 1300 °C. Thus, on the one hand, the mullite phase is consumed yielding cordierite, and on the other hand, it is formed again by the reaction of alumina and silica in the presence of a liquid phase. The presence of cristobalite can be associated with the crystallization of the amorphous silica at sufficiently high temperatures, while the spinel formation can be explained by the reaction between alumina (which is in excess in the precursor mixture) and proto-enstatite at temperatures between 1200 and 1250 °C [42].

Additionally, the formation of liquid phase in the system could have occurred at a temperature below the eutectic point of the phase equilibrium diagram (1355 °C) due to the presence of impurities derived from the raw materials which may form low-melting phases. Therefore, at the highest temperature, proto-enstatite grains could have been decomposed and dissolved into the siliceous liquid, thereby continuing to generate cordierite by a reaction between mullite and the liquid phase. Although the alumina content determined in the samples treated at 1330 °C by the Rietveld method did not decrease compared to that determined in samples heated at 1300 °C, the participation of residual alumina in the formation of the cordierite phase cannot be ruled out.

On the other hand, local crystallization of sapphirine can occur at temperatures lower than 1320 °C [40]. Its decomposition into spinel and a liquid phase could explain the increase of the content of the former phase that was recorded after thermal treatment at 1330 °C. Even though the liquid phase content would be increased by this reaction, the subsequent reaction of this liquid with mullite would explain the decrease in the glass phase amount at 1330 °C.

3.2. Microstructural characterization of porous cordierite-based materials

The open ($\%P_{open}$) and total ($\%P_{total}$) porosity values of disks treated at 1275, 1300 and 1330 °C for 4 h are shown in Table 3.

According to these results, the open and total porosities of disks consolidated with corn starch were significantly lower than those of disks prepared with potato starch (42–46% and 46–49% compared to 49–55% and 50–56%, respectively). For both starting systems, these porosities decreased slightly when the T_s increased from 1275 °C up to 1330 °C. The decrease in open porosity with increasing T_s is not too surprising. Moreover, the transient content of the liquid phase and even its fluidity—and thus the degree of pore closure—are expected to

Table 3
Open porosity ($\%P_{open}$) and total porosity ($\%P_{total}$) values of disk-shaped samples sintered at 1275, 1300 and 1330 °C for 4 h.

Porosity	PM-potato			PM-corn		
	1275 °C	1300 °C	1330 °C	1275 °C	1300 °C	1330 °C
P_{open} (%)	55 ± 1	54 ± 5	49 ± 4	46 ± 7	43 ± 5	42 ± 3
P_{total} (%)	56 ± 3	55 ± 4	50 ± 4	49 ± 7	45 ± 4	46 ± 4

increase. Nevertheless, in the case of cordierite-based ceramics, this finding is not trivial because, depending on the composition, it is well-known that siliceous liquid phases of the system Al_2O_3. SiO_2. MgO can present a poor wetting (high contact angle), mainly on cordierite and even more on mullite, and may thus lead to swelling instead of densification [43]. As for the closed porosity, the samples prepared with potato starch exhibited lower values (~ 1%) than those prepared with corn starch (2–4%) for all sintering temperatures. The low amount of closed pores is typical for materials prepared by the SCC method because in this process starch is not just a pore former (with starch granules as transient spacers); in fact, the starch granules swell and gelatinize into an amorphous mass (the starch gel), which intrudes into the interparticle voids and thus generates mainly open porosity.

Based on these results and taking into account the porosity values for green disks before the starch burnout (38 ± 6% and 36 ± 5% for disks formed with potato and corn starch, respectively) and the estimated porosity values after considering all the starch was removed by burnout (~ 62% and ~ 64%, respectively), the degree of densification achieved for the samples consolidated with corn starch is much higher than that attained for samples formed with potato starch (especially those sintered at the lower temperatures, 1275 and 1300 °C).

The total porosity values obtained for the samples prepared with corn starch were in the range of those reported for porous ceramic materials processed by the starch consolidation casting (SCC) method with a similar percentage of starch [30,44]. It is well known that the porosities generated in materials shaped by SCC are higher than the nominal starch content (39 vol%) due to the swelling experienced by the starch granules during the thermal consolidation process. Moreover, since the swelling capacity depends on the starch type, the porosity of the disks is influenced by the type of starch. In general, potato starch has a higher swelling capacity and swelling velocity than corn starch [45,46]. However, it has to be considered that the swelling can be counterbalanced by steric effects (excluded-volume effect) which limit this process. In addition, as reported in our previous paper [47], the features of the developed pre-firing microstructures are significantly influenced by the advance of the gelatinization process; therefore, the different behavior of the materials prepared with potato and corn starches during the thermal treatments could be explained taking into account this parameter. Thus, the occurrence of a more advanced gelatinization process in the majority of starch granules can lead to their loss of integrity, particularly in the case of the potato starch, because the consolidation temperature for the PM-potato system was higher than its $T_{G'max}$ (temperature at which the storage modulus value in an oscillatory rheological test is maximum). In addition, the diffusion of amylose (i.e. the low-molecular weight fraction leached out from the starch granules) into the matrix interstices (interparticle voids) implies that the original starch granules are transformed into a continuous and amorphous gel mass [48]. The combined effect of the above-mentioned factors determined the development of a small amount of cavities, particularly in the materials formed with potato starch. Moreover, the presence of a high amount of amorphous gel mass in the matrix interstices could lead to the development of a high amount of interstitial porosity after burnout of the organic components, and in consequence, to a lower degree of matrix densification after sintering.

Based on these results, it was concluded that the type of starch used for forming the disks, and in a much lesser extent, the reaction-sintering temperature (T_s), were the main factors determining the evolution of porosity during the thermal treatments of the materials.

Typical SEM images of fracture surfaces of samples sintered at 1275, 1300 and 1330 °C for 4 h are shown in Figs. 2–4, respectively.

According to the SEM images, the microstructures developed after thermal treatments carried out at the different temperatures showed that the porosity was associated with large convex cavities (cells) embedded in the cordierite-based matrix, which were mainly generated by the removal of native starch granules with certain structural integrity, and with much smaller pore channels or throats (cell windows) interconnecting these cavities. In all materials, the cavities presented a certain degree of tortuosity and nonspecific morphology, especially when the treatment temperature was lowest (1275 °C), but their size was primarily determined by the native starch type used in the thermal consolidation. The removal of potato starch produced cavities with the greatest size, in agreement with the fact that their dimensions are related to dry starch granule sizes or those having suffered some degree of swelling. In addition, larger cavities generated by the joining of various cavities were also observed, as reported in our previous paper [47]. Of course, the relatively small differences determined between the open porosity values exhibited by the materials prepared with potato or corn starch, respectively, and sintered at different temperatures (Table 3), were not visible at first in the SEM images (Figs. 2–4) because they were masked by the microstructural heterogeneity.

The microstructural features of the matrix developed at each temperature were similar for both types of materials (materials prepared with corn starch and potato starch). With regard to the ceramic matrix developed in the materials sintered at 1300 °C (Fig. 5a), which was similar to those developed after treatment at 1275 °C, the small particle sizes and their irregular morphological characteristics indicate that the

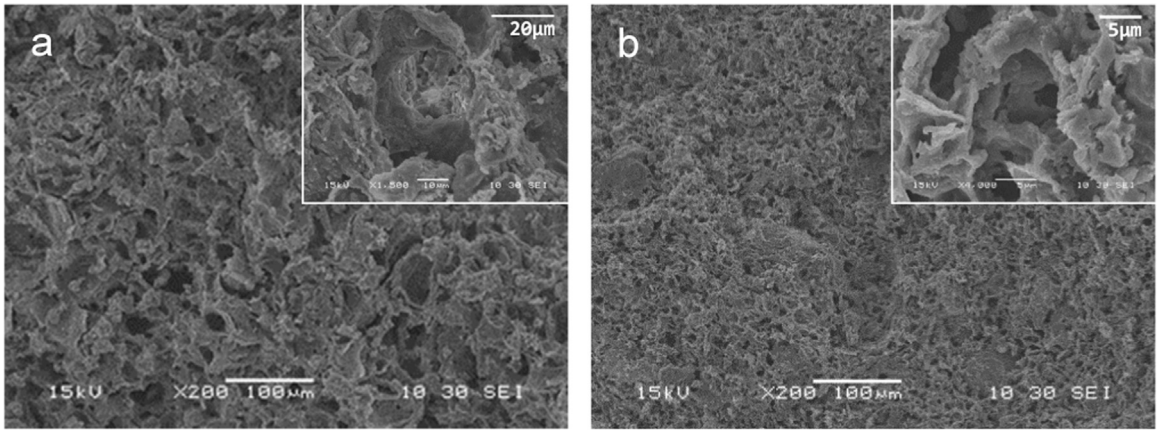

Fig. 2. SEM images of the microstructures developed at 1275 °C, 4 h (fracture surfaces) for materials formed with potato starch (a) and corn starch (b).

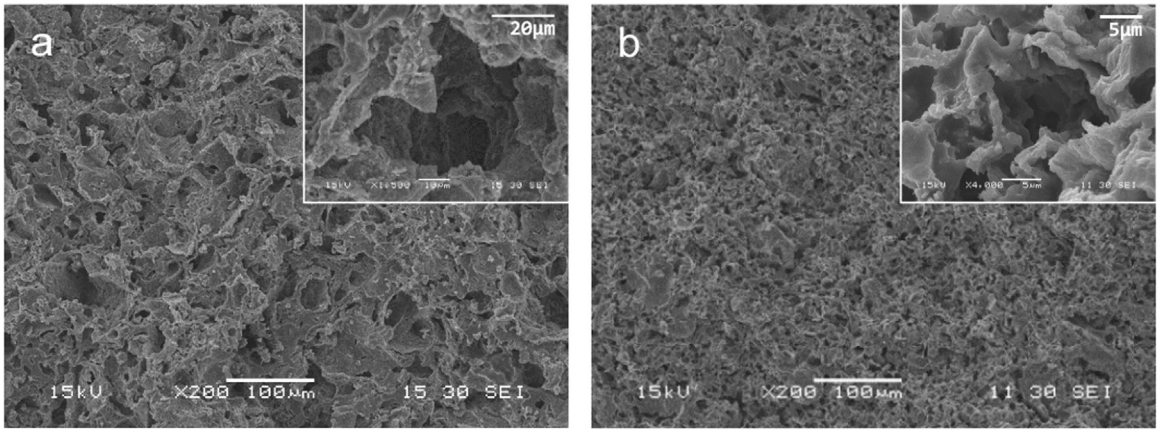

Fig. 3. SEM images of the microstructures developed at 1300 °C, 4 h (fracture surfaces) for materials formed with potato starch (a) and corn starch (b).

degree of sintering (formation of solid necks) achieved at these temperatures was not very high. Contrarily, the matrices developed in the samples treated at 1330 °C (Fig. 5b) reached a greater degree of cohesion than those treated at lower temperatures. Thus, the development of solid necks between particles was really evident only when the temperature increased up to 1330 °C. Moreover, the higher degree of densification achieved for the material at 1330 °C was enabled by the high temperature, together with the presence of phases based on silicates with low melting points, which facilitate material transport, thus increasing the densification rate. In these materials, the growth of elongated mullite grains (< 3 µm of length) with an aspect ratio ~ 3 can be associated with the occurrence of the mullitization reaction in the presence of a liquid phase. Besides this type of grain, equiaxial grains with an aspect ratio ~ 1 were also observed.

Also, taking into account pores bigger than the grain size, which are embedded in the ceramic matrix containing small pores and do not contribute to the shrinkage of the body, the volume shrinkage of the disks treated at all temperatures (~ 30%) can be assumed to correspond exclusively to the densification of the matrix.

The results of stereology-based image analysis are shown in Table 4. The pore size, or more precisely the characteristic length of the pore space heterogeneity, here quantified via the mean chord length, was larger (24–31 µm) for the materials prepared with potato starch than for those prepared with corn starch (15–21 µm). That signifies, as expected, that there is a clear difference between materials prepared with the two starch types, in agreement with the fact that their original granules have different sizes, although for potato starch the results listed in Table 4 do not reveal a clear trend with firing temperature (the sample prepared with potato starch and sintered at 1330 °C showed exceptionally large pores and large matrix regions between them, obviously due to the coalescence of these large pores when the viscosity of the liquid melt became sufficiently low). It has to be emphasized that for spherical and other isometric convex pores (cavities) the mean chord length is always significantly smaller than the pore diameter (or equivalent diameter), while for non-convex pores like pore channels (throats), concave pores or pores with anisometric or irregular shapes, e.g. coalesced pores, this statement does not apply (because a pore diameter is not uniquely defined in this case). On the other hand, both types of starch granules undergo swelling during this process, which generally tends to increase the size of the starch granules, and after starch burnout both types of pores (i.e. those from potato starch and corn starch) undergo shrinkage during sintering. Furthermore, due to the higher swelling factor of potato starch compared to corn starch, the loss of integrity and rupture experienced by the potato starch granules can be larger than that experienced by the corn starch granules during the thermal consolidation process, which could explain the lower values obtained for mean chord lengths in the materials prepared with potato starch compared to the original granule size (Table 1). It is thus clear that there are basically several counteracting effects in both cases that may compensate each other, a situation that is further complicated by the aforementioned liquid melt forming reactions and the change of the liquid melt viscosity with temperature. Similar differences as to the mean chord lengths have been confirmed for the mean pore distance, i.e. the mean chord length of the matrix between the large pores resulting from starch burnout: the mean distance between pores is much larger for samples prepared with potato starch (11–19 µm), than for samples prepared with corn starch (7–8 µm). The reason is evident: potato starch granules are larger than corn starch granules and therefore a smaller amount of them is needed to achieve comparable or even higher porosities. Consequently, the mutual distance of the pores after

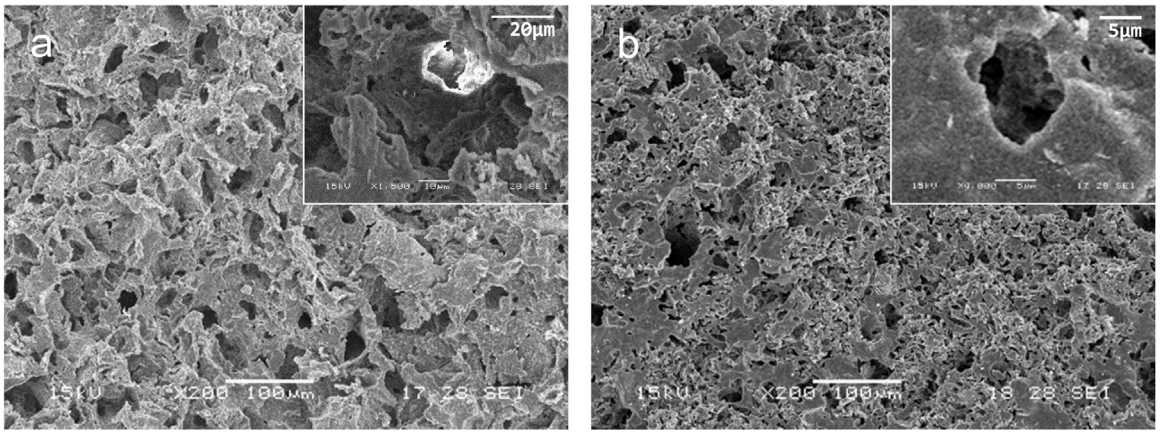

Fig. 4. SEM images of the microstructures developed at 1330 °C, 4 h (fracture surfaces) for materials formed with potato starch (a) and corn starch (b).

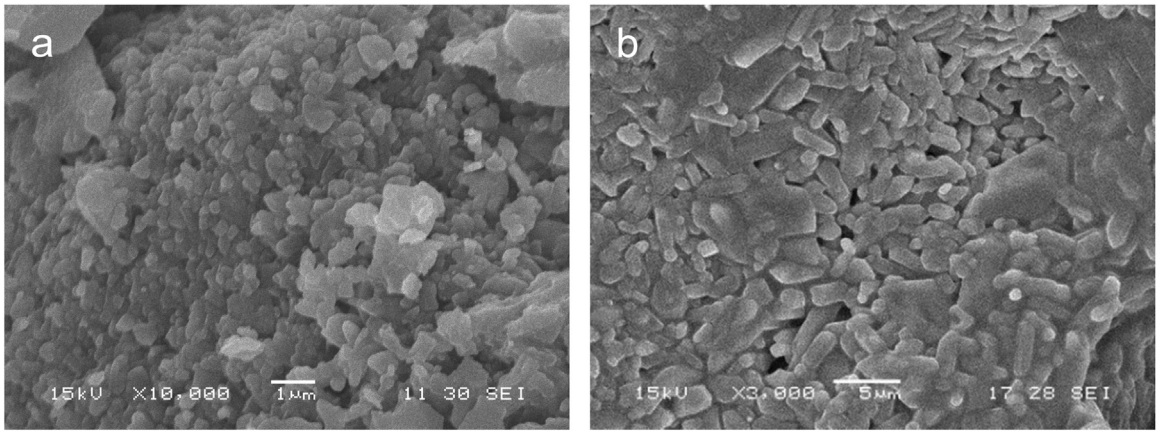

Fig. 5. Typical ceramic matrices developed in materials treated at 1300 °C (a) and 1330 °C (b), 4 h.

sintering is also larger when potato starch is used. The mean pore distance increases slightly with increasing T_s for both types of samples, but this increase is close to negligible unless coalescence phenomena come into play as in the aforementioned case of the sample prepared with potato starch and sintered at 1330 °C.

With regard to the surface density, which is related to the specific surface of the pores and thus to the starch granules from which these pores were formed, the values obtained for the materials prepared with potato starch (86–110 mm^{-1}) and corn starch (149–181 mm^{-1}) are in agreement with the fact that the smaller the size of the pores and starch granules are, the higher the surface density is. The mean curvature integral density, whose values were 912–2782 mm^{-2} and 2373–2945 mm^{-2} for samples prepared with potato and corn starch respectively, is a measure of the curvature per unit volume that is high when the curvature is high, which is the case not only when the pores are small, but also when local high-curvature regions are present, as in the case of coalesced pores. This explains the surprisingly high value of this parameter for the aforementioned case of the sample prepared with potato starch and sintered at 1330 °C.

The pore size distributions (cumulative curves) of materials sintered at 1330 °C obtained by mercury intrusion porosimetry are shown in Fig. 6. The pore sizes measured in both materials were much smaller than the cavity sizes observed in SEM images and determined via image analysis from optical micrographs, as expected based on the characteristics of the developed pores: large cavities interconnected by pore channels or throats of much lower size. The mercury intrusion results are then attributed to the "bottle neck" effect that occurs when mercury accesses a large cavity through a narrow channel [49]. Thus, the pore diameters determined by mercury porosimetry correspond to the pore throat sizes [50]. The median pore sizes (D_{50}) for materials prepared with the potato and corn starches were 10.4 and 4.6 μm, respectively. These values indicate that the starch type used also influenced the pore throat size. A similar dependence was also observed in porous mullite materials prepared by using native starches [47]. On the other hand, the obtained range of pore throat sizes was rather similar to those reported in previous work [18] for similar ceramic materials prepared by the SCC method using Argentinean native starches (potato, corn and cassava) or modified potato starch.

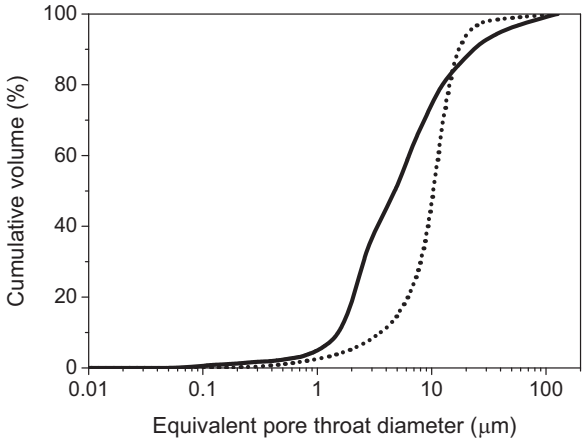

Fig. 6. Pore size distributions (cumulative curves) measured via mercury porosimetry for materials formed with potato starch (dotted curve) and corn starch (solid curve) sintered at 1330 °C.

According to the frequency curves obtained from mercury porosimetry measurements of samples after sintering the content of interstitial matrix pores, i.e. interparticle voids with sizes typically < 0.5 μm (as reported in earlier studies for oxide ceramics prepared by SCC [30,51]), are very small for the ceramics after sintering (evidently due to the presence of the liquid melt phase that tends to close these small pores) and similar for the materials prepared with both types of starch.

Based on the phases generated after the burnout of organics (removal of starch and processing additives) and sintering treatments of the bodies at 1275, 1300 and 1330 °C, and the degree of densification of the ceramic matrix achieved in each case, the highest temperature (1330 °C) was selected as a suitable thermal treatment condition for preparing porous cordierite-based materials for mechanical evaluation.

Table 4
Microstructural characteristics determined via image analysis for porous cordierite in this work (errors in this table correspond to 95% confidence intervals).

Microstructural feature	PM-potato			PM-corn		
	1275 °C	1300 °C	1330 °C	1275 °C	1300 °C	1330 °C
Mean chord length (μm)	26.9 ± 3.9	24.1 ± 2.4	30.8 ± 6.3	21.1 ± 4.0	15.8 ± 3.1	15.3 ± 3.1
Mean pore distance (μm)	10.7 ± 1.6	12.6 ± 1.3	18.6 ± 3.8	6.7 ± 1.3	7.9 ± 1.6	8.2 ± 1.7
Surface density (mm^{-1})	109 ± 12	110 ± 12	86 ± 13	149 ± 23	181 ± 26	172 ± 25
Mean curvature integral density (mm^{-2})	912 ± 72	1884 ± 152	2782 ± 281	2945 ± 313	2863 ± 271	2373 ± 234

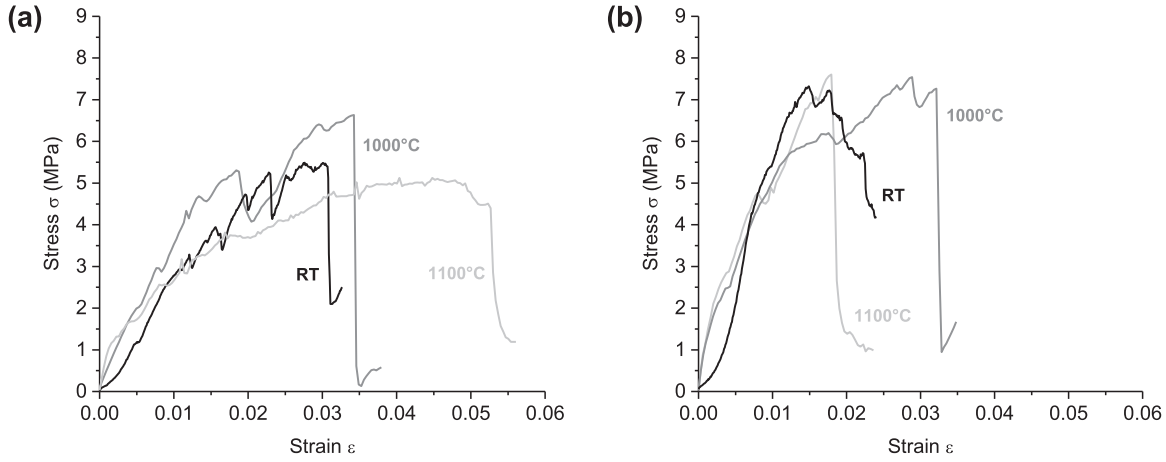

Fig. 7. Typical stress-strain curves of porous cordierite disks (T_s = 1330 °C) prepared from PM-potato (a) and PM-corn (b) systems.

3.3. Mechanical behavior as a function of temperature

Typical stress-strain curves determined in diametral compression tests at room temperature (RT) and high temperatures for porous cordierite disks consolidated with different starches and sintered at 1330 °C, are presented in Fig. 7. The values for the mechanical parameters are reported in Table 5.

The stress-strain curves of sintered disks determined at RT have a region of linear elastic deformation (dismissing the first concave part of the RT curves which is due to the accommodation of the sample-loading system), and then they deviate from linearity as is evidenced by the relatively low values of σ_Y/σ_F (< 60%). From a phenomenological point of view, the irreversible deformation mechanism leading to this deviation is microcracking, similar to what occurred with green compacts [26]. However, the underlying micromechanism is different because, for instance, the fracture is inter-particle in the green state and intergranular or transgranular (intragranular) in the sintered specimens, and the plasticity provided by the organic binder is absent in the latter. As is well known, porous materials like ceramic foams can exhibit quasi-plastic behavior, although their microstructural elements (struts in open-cell foams, walls in closed-cell foams and highly porous materials) are completely brittle [52]. Microcracking is certainly associated to the failure of these microstructural elements, which is facilitated by the presence of a large amount of pores.

Typical fractured cordierite disks tested at room and high temperatures are shown in Fig. 8.

In both cases, the disks tested at RT showed a diametral fracture, which validates the obtained strength values [36]. Such failure is evidenced in the stress-strain (σ-ε) curves (Fig. 7) as a sudden drop in stress, corresponding to the propagation of the diametral crack. The additional damage by fragmentation in the contact region where the disks were loaded was mainly observed in the disks prepared with corn starch (Fig. 8b).

From the fracture mechanics relationship between K_{IC} (critical stress intensity factor or fracture toughness) and σ_F:

$$K_{IC} = \sigma_F Y c^{1/2} \quad (3)$$

where Y is a factor which depends on the critical defect geometry, the critical defect size c can be estimated. Considering $K_{IC} \sim 2.2$ MPa m$^{1/2}$ and $\sigma_F \sim 245$ MPa for a dense cordierite material [53], the flaw sizes calculated range between 20 μm and 40 μm, for Y varying from 2.0 (for a shallow elliptical defect) to 1.4 (for a semi-elliptical flaw) [54], respectively. Taking this calculation as a rough and conservative estimate of the critical defect size of cordierite material (in our case, the presence of other phases, mainly the silicate glass phase, must surely reduce values of K_{IC}, σ_F and c), the cavities observed by SEM can be considered as critical flaws determining the mechanical resistance sintered at 1330 °C, bearing in mind their sizes as estimated by stereological analysis (Table 4). Furthermore, assuming the same values of K_{IC} and Y factor for both cordierite disks (those prepared with potato starch and those prepared with corn starch), the following ratios between the strengths and defect sizes of the two types of materials can be established:

$$\frac{\sigma_{F(PM-potato)}}{\sigma_{F(PM-corn)}} \cong \frac{c_{(PM-corn)}^{1/2}}{c_{(PM-potato)}^{1/2}} \quad (4)$$

Using the mean values of pore sizes (Table 4) for $c_{(PM\text{-}corn)}$ and $c_{(PM\text{-}potato)}$ and mechanical strengths (Table 5), a similar ratio is obtained for both parameters, approximately 1.4 and 1.5, respectively. Thus, the lower values for mechanical strength and apparent Young's modulus at RT determined for the disks prepared with potato starch and sintered at 1330 °C can be attributed to its higher porosity, larger pores (cavities) and, as mentioned earlier, the larger degree of heterogeneity of this sample, which has been discussed above. On the other hand, the lower strain to failure displayed by the specimens prepared with corn starch correlates well with their higher stiffness.

When both types of cordierite disks were tested at 1000 °C, the stress-strain curves (Fig. 7) were similar to those obtained in the tests at RT, although the deviation from linear response occurred at a higher stress level, as shown by the increase of the σ_Y/σ_F ratio (Table 5), with the non-linearity being larger in the case of disks formed with potato

Table 5
Mechanical parameters of porous cordierite disks (T_s = 1330 °C) tested at different temperatures.

Testing temperature	System	E_a (GPa)	σ_F (MPa)	ε_F	σ_Y (MPa)	σ_Y/σ_F (%)
RT	PM-potato	0.40 ± 0.06	5.3 ± 0.4	0.023 ± 0.009	2.4 ± 0.1	47 ± 2
	PM-corn	0.90 ± 0.09	7.9 ± 0.3	0.016 ± 0.006	4 ± 1	46 ± 17
1000 °C	PM-potato	0.40 ± 0.01	7.1 ± 0.5	0.032 ± 0.003	4.4 ± 0.1	62 ± 6
	PM-corn	0.50 ± 0.05	6.6 ± 0.9	0.029 ± 0.005	4.6 ± 0.4	55 ± 7
1100 °C	PM-potato	0.70 ± 0.01	4.6 ± 0.7	0.036 ± 0.015	4.4 ± 0.1	22 ± 4
	PM-corn	0.90 ± 0.30	9 ± 2	0.022 ± 0.006	2.4 ± 0.4	26 ± 2

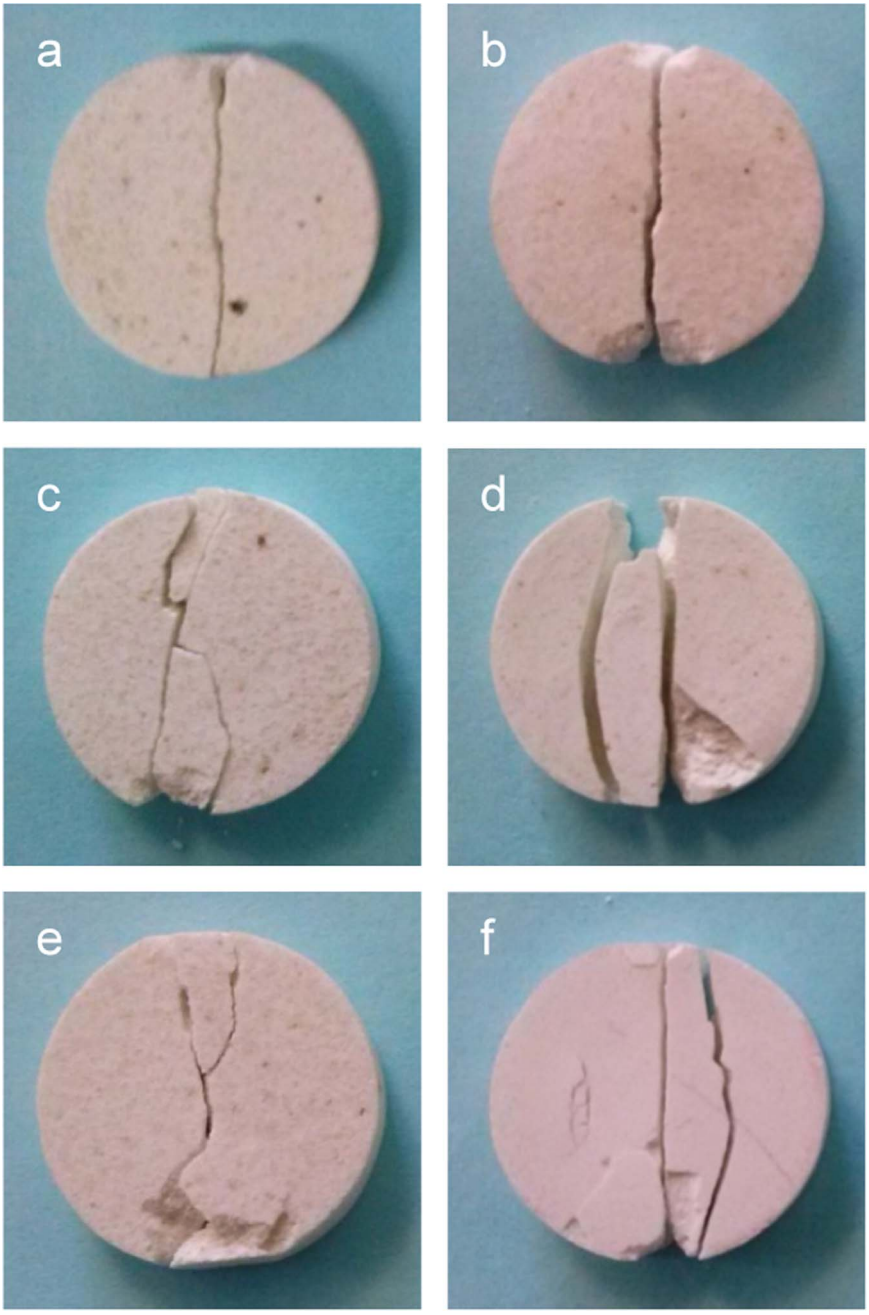

Fig. 8. Typical fracture patterns of porous cordierite disks (T_s =1330 °C) tested at RT (a: PM-potato; b: PM-corn), 1000 °C (c: PM-potato; d: PM-corn) and 1100 °C (e: PM-potato; f: PM-corn).

starch. At this temperature, fracture strength and pore size values do not follow Eq. (4) at all, which indicates that at this temperature there are other factors affecting the mechanical behavior of the porous cordierite-based materials. The main reason is the presence of the silicate glassy phase that softens at temperatures below 1000 °C. Also, the shape of stress-strain curves obtained at 1100 °C clearly indicates that a low-viscosity phase affected the mechanical behavior of disks: an early and significant deviation of the linear behavior is displayed, having the lowest σ_Y/σ_F ratios in the range of testing temperatures. Again, the ratio between σ_F of both types of cordierite disks is quite different from that predicted by Eq. (4), which is based on mean pore sizes. Nevertheless, the σ-ϵ curves of specimens prepared with corn starch resemble those determined at RT.

In addition to an irregular diametral fracture, further fragmentation of the disks occurred when they were mechanically tested at 1000 °C (Fig. 8). This is responsible for the small drops in stress displayed in the stress-strain curves (Fig. 7) until diametral failure occurred with an abrupt and pronounced reduction of the stress. Moreover, the typical fracture pattern at 1100 °C was also diametral with secondary cracking (Fig. 8); in some cases, permanent deformation (flattening) was evident in the contact zone, especially in those disks obtained by the PM-potato system, as a consequence of the irreversible deformation resulting from the silicate viscous phase.

The variation in parameters σ_F and E_a between RT and 1000 °C was not very significant or, as was expected, they decreased due to the presence of the viscous silicate glassy phase. The exception to this behavior is the mechanical strength of disks prepared with potato starch, which is the material with greater porosity; in this case, the strength is slightly higher at 1000 °C than at RT. In spite of the presence of a greater amount of viscous phase with higher fluidity at 1100 °C (compared to 1000 °C), an unexpected increase in the apparent modulus and strength in materials prepared with the PM-potato and PM-corn systems, respectively, was determined.

Before discussing this particular behavior, it is worth noting that

when the contact area between the disks and the platens becomes flatter, the stress generated in the center of disks tends to decrease, and the slope of the load vs. displacement curve tends to increase [35]. As a result, the use of the Hertz equation (Eq. (1)) for stress calculation overestimates its value, which is translated to the stress-strain curve, its slope and the calculated apparent Young's modulus. Furthermore, the disk flattening (which likely occurs during heating) also reduces the diametral displacement of the actuator, i.e. the value of d in Eq. (2), which decreases disk deformation ε and increases the calculated parameter E_a. For this reason, the value of E_a at 1100 °C when the flatness of tested disks occurred, is considered fictitious, being actually overestimated. Furthermore, σ-ε curves displayed only a small degree of linearity, which represents another source of uncertainty. This restriction makes any discussion concerning the apparent increase of E_a when mechanical testing was performed at 1100 °C highly problematic.

In order to explain the unexpected increase of mechanical strength at high temperature, the role of the silicate glassy phase has to be considered. On the one hand, the softening of the silicate glassy phase present in the porous cordierite-based materials studied here facilitates the displacement and rearrangement of particles by viscous flow and finally, the failure of the specimen. In principle, this irreversible deformation should add to microcracking as mechanisms linked to the non-linearity of the stress-strain curves. On the other hand, however, the presence of a low-viscosity phase also hinders microcrack propagation by tip blunting [55]. Furthermore, the applied stresses can be relieved by the irreversible deformation of this viscous phase itself. Either of the last two phenomena reduces the stress supported by the material (positive effects on mechanical bearing capacity), opposing the (negative) effect of the viscous phase supporting fracture via particle sliding. Which of these effects caused by the presence of a viscous phase dominates the mechanical behavior depends on several factors, mainly the fluidity of the viscous phase, the distribution of this phase in the microstructure and the size of the microcracks. In relation to these factors, the displacement of the viscous phase could be restricted by small interstitial pores and windows in the porous matrix which act as "bottle necks". This occlusion will be more effective for smaller and less interconnected pores.

Thus, in the case of the disks prepared with corn starch, the recovery of mechanical strength at 1100 °C (after a slightly decrease at 1000 °C) can be attributed to the highly efficient occlusion of the low viscosity phase by the small windows and less interconnected pores (defining the ratio P_{open}/P_{total} as the interconnection degree, the values for disks prepared using potato or corn starches were 0.98 and 0.91, respectively), which reduced its effects on the sliding of particles which eventually led to the material's fracture. Other positive effects such as microcrack tip blunting and/or stress relief by the irreversible deformation of the silicate viscous phase could also exist. This last process could explain the strong non-linear σ-ε behavior for this thermal condition. Conversely, the larger windows and more-connected pores in the material prepared from the PM-potato system were not effective to impede the fluid phase displacement, as is manifest also in the shape of the stress-strain curve, and the value of σ_F decreased between 1000 and 1100 °C.

The increase in the value of σ_F for disks prepared with potato starch between RT and 1000 °C, as well as the small decrease in this mechanical parameter in those specimens formed by PM-corn system, cannot be explained using the same arguments. The viscous silicate phase movement seems to be restricted by the lower fluidity of the silicate viscous phase at 1000 (compared to 1100 °C). An indication of this restriction is the higher linear proportion of stress-strain curves at 1000 °C (the highest σ_Y/σ_F were calculated for 1000 °C, see Table 5). In this situation, occlusion by the little holes (windows) was not the dominant effect on the mechanical behavior of the porous cordierite-based materials. On the other hand, a plausible hypothesis is that the characteristics of the microcracks (size, tip sharpness, etc.) present in the matrix of both types of disks (prepared from PM-potato or PM-corn systems) are different, as is the porosity generated with potato or corn starches. Thus, it could be possible that the main determining factor is microcrack tip blunting, which would be more efficient in specimens prepared with potato.

In comparison with previous results obtained for porous cordierite-based materials prepared by SCC using a precursor mixture with the same proportions of alumina, talc and kaolin as those used in this work, and native potato and corn starches (from Argentina) [17], the present materials displayed some differences in the high temperature mechanical response. These cordierite materials exhibited superior performance, especially at 1100 °C, although they were more brittle in spite of the contribution of the glass phase to softening and displayed higher values of the basic mechanical parameters (σ_F and E_a). Taking into account the similarities in porosities and microstructural features between the first set of cordierite disks and those studied in the present work, the superior mechanical behavior of the latter is attributed to differences in the characteristics of the raw materials (mainly impurities), which led to a distinct mineralogical composition and glass phase nature, among other aspects. The presence of mullite, for instance, in the porous disks in this work could be a decisive factor behind the higher values for their high-temperature mechanical parameters.

4. Conclusions

In this work, porous cordierite ceramics with two types of microstructures were prepared by starch consolidation casting using native potato and corn starch and sintered at three different temperatures.

The XRD results showed that with increasing sintering temperature, the cordierite content increases from 27% to 59%, while the contents of all other phases (except for spinel, whose content is very low, viz. 1–4%) have significantly lower values after sintering at 1330 °C (compared to 1275 °C). Apart from cordierite and a significant amount of glass phase (15–18%), the main phases are mullite (15–19%) and alumina (5–14%). The total porosities are in the overall range of 45–56% (46–50% for samples sintered at 1330 °C), while open porosities are in the overall range of 42–55% (42–49% for samples sintered at 1330 °C). In all cases, the materials prepared with potato starch have higher porosity than those prepared with the same amount of corn starch, evidently mainly because of the higher degree of swelling of the potato starch granules. Microscopic investigation by SEM confirmed much a larger pore size for the materials prepared with potato starch compared to those prepared with corn starch. A quantification of these findings via image analysis resulted in a mean chord length of 24–31 μm for the materials prepared with potato starch and 15–21 μm for those prepared with corn starch. Corresponding differences between the two starch types have been confirmed for the mean pore distance (with potato starch 11–19 μm, and corn starch 7–8 μm), the surface density (with potato starch 86–110 mm^{-1}, and corn starch 149–181 mm^{-1}) and the integral mean curvature density (with potato starch 912–2782 mm^{-2}, and corn starch 2373–2945 mm^{-2}). In addition, the pore throat size measured via mercury porosimetry is much larger for the former than for the latter, as expected. The mechanical behavior of porous cordierite ceramic disks in diametral compression is rather complex, especially at high temperatures (1000 and 1100 °C) and has been discussed in great detail. In summary, it may be concluded that—mainly due to higher porosity—materials prepared with potato starch tend to have a lower apparent Young's modulus, lower elastic limit and lower mechanical strength than those prepared with corn starch. At high temperatures the basic mechanical properties (strength and elastic modulus) are surprisingly high despite the presence of a silicate glassy phase due to the particular combination of the porous microstructure features.

Acknowledgements

The authors gratefully acknowledge Dra. P. Pena and Ms. M. Rubio of the Institute of Ceramics and Glass, CSIC, Madrid, Spain for

accomplishing the measurements of pycnometric densities of the cordierite precursor mixture used in this work. This study was funded by MINCyT (Argentina) – MEYS (Czech Republic) under project ARC/11/06 (Argentina) – 7AMB12AR015 (Czech Republic).

References

[1] E.S. Rao, P. Manohar, Effect of particle size on high purity cordierite for kiln furniture applications, J. Ceram. Process. Res. 17 (2016) 448–453.
[2] S. Sembiring, W. Simanjuntak, R. Situmeang, et al., Preparation of refractory cordierite using amorphous rice husk silica for thermal insulation purposes, Ceram. Int. 42 (2016) 8431–8437.
[3] I. Jankovic-Castvan, S. Lazarevic, B. Jordovic, et al., Electrical properties of cordierite obtained by non-hydrolytic sol-gel method, J. Eur. Ceram. Soc. 27 (2007) 3659–3661.
[4] D. Fino, V. Specchia, Open issues in oxidative catalysis for diesel particulate abatement, Powder Technol. 180 (2008) 64–73.
[5] J.K. Park, J.S. Lee, S.I. Lee, Preparation of porous cordierite using gel casting method and its feasibility as a filter, J. Porous Mater. 9 (2002) 203–210.
[6] Y. Dong, X. Liu, Q. Ma, et al., Preparation of cordierite-based porous ceramic microfiltration membranes using waste fly ash as the main raw materials, J. Membr. Sci. 285 (2006) 173–181.
[7] M.A. Ulla, R. Mallada, J. Coronas, et al., Synthesis and characterization of ZSM-5 coatings onto cordierite honeycomb supports, Appl. Catal. A: Gen. 253 (2003) 257–269.
[8] M. Majumder, S. Mukhopadhyay, O. Parkash, et al., Sintering and crystallization behaviour of chemically prepared cordierite for application in electronic packaging, Ceram. Int. 30 (2004) 1067–1070.
[9] M.A. Camerucci, G. Urretavizcaya, A.L. Cavalieri, Mechanical behavior of cordierite and cordierite-mullite materials evaluated by indentation techniques, J. Eur. Ceram. Soc. 21 (2011) 1195–1204.
[10] M.A. Camerucci, G. Urretavizcaya, M.S. Castro, et al., Electrical properties and thermal expansion of cordierite and cordierite-mullite materials evaluated by indentation techniques, J. Eur. Ceram. Soc. 21 (2001) 2917–2923.
[11] A.G. Tomba Martínez, M.A. Camerucci, A.L. Cavalieri, Indentation crack profiles of cordierite materials under mechanical and thermal biaxial stresses, J. Eur. Ceram. Soc. 26 (2006) 2527–2531.
[12] A. Shyam, G. Bruno, T.R. Watkins, et al., The effect of porosity and microcracking on the thermomechanical properties of cordierite, J. Eur. Ceram. Soc. 35 (2015) 4557–4566.
[13] L. Zhang, S. Olhero, J.M.F. Ferreira, Thermo-mechanical and high-temperature dielectric properties of cordierite-mullite-alumina ceramics, Ceram. Int. 42 (2016) 16897–16905.
[14] N. Obradovic, S. Filipovic, N. Dordevic, et al., Effects of mechanical activation and two-step sintering on the structure and electrical properties of cordierite-based ceramics, Ceram. Int. 42 (2016) 13909–13918.
[15] H.M. Alves, G. Tarí, A.T. Fonseca, J.M.F. Ferreira, Processing of porous cordierite bodies by starch consolidation, Mater. Res. Bull. 33 (1998) 1439–1448.
[16] F. Manabu, N. Masayuki, Y. Yoshizawa, Fabrication and properties of ultra-highly porous cordierite with oriented micrometer-sized cylindrical pores by gelation and freezing method, J. Ceram. Soc. Jpn. 116 (2008) 1322–1325.
[17] M.L. Sandoval, M.H. Talou, A.G. Tomba Martínez, et al., Mechanical testing of cordierite porous ceramic using high-temperature diametral compression, J. Mater. Sci. 45 (2010) 5109–5117.
[18] M.L. Sandoval, M.A. Camerucci, A.G. Tomba Martínez, High-temperature mechanical behavior of cordierite-based porous ceramics prepared by modified cassava starch thermogelation, J. Mater. Sci. 47 (2012) 8013–8021.
[19] Z. Fu, J. Xie, F. He, et al., Synthesis of porous cordierite and application for MnO_x/TiO_2 catalyst support, Russ. J. Appl. Chem. 87 (2014) 1749–1754.
[20] Y. Li, W. Cao, J. Feng, et al., Fabrication of cordierite foam ceramics using direct foaming and slip casting method with plaster molds, Adv. Appl. Ceram. 114 (2015) 465–470.
[21] Y. Li, W. Cao, L. Gong, et al., Properties of highly porous cordierite ceramic obtained by direct foaming and gel casting method, Ceram. Silik. 60 (2016) 91–98.
[22] Y. Kobayashi, K. Sumi, E. Kato, Preparation of dense cordierite ceramics from magnesium compounds and kaolinite without additives, Ceram. Int. 26 (2000) 739–743.
[23] M.A. Camerucci, G. Urretavizcaya, A.L. Cavalieri, Sintering of cordierite based materials, Ceram. Int. 29 (2003) 159–168.
[24] E. Gregorová, W. Pabst, A. Musilová, et al., High-temperature elastic properties of ceramics in the system MgO-Al_2O_3-SiO_2 measured by impulse excitation, Key Eng. Mater. 592–593 (2014) 696–699.
[25] C.W. Sinton, Raw Materials for Glass and Ceramics – Sources, Processes, and Quality Control, 1st ed., John Wiley, Hoboken, N. J., 2006.
[26] M.L. Sandoval, M.H. Talou, A.G. Tomba Martínez, et al., Starch consolidation casting of cordierite precursor mixtures-rheological behavior and green body properties, J. Am. Ceram. Soc. 98 (2015) 3014–3021.
[27] M.H. Talou, Procesamiento de materiales cerámicos porosos de mullita por consolidación directa con almidón (Processing of porous mullite ceramic by starch direct consolidation), National University of Mar del Plata, Mar del Plata, 2012 (Ph.D. Thesis).
[28] R. Barea, M.I. Osendi, P. Miranzo, et al., Fabrication of highly porous mullite materials, J. Am. Ceram. Soc. 88 (2005) 777–779.
[29] M.H. Talou, M.A. Camerucci, Two alternative routes for starch consolidation of mullite green bodies, J. Eur. Ceram. Soc. 30 (2010) 2881–2887.
[30] W. Pabst, E. Gregorová, I. Sedlářová, et al., Preparation and characterization of porous alumina-zirconia composite ceramics, J. Eur. Ceram. Soc. 31 (2011) 2721–2731.
[31] J. Rodríguez-Carvajal, Recent developments of the program FULLPROF, Commission on Powder Diffraction (IUCr), Newsletter 26 (2001) 12–19.
[32] M.S. Conconi, N.M. Rendtorff, E.F. Aglietti, Evaluation of non-crystalline phase in AZS refractories by XRD methods, New J. Glass Ceram. 1 (2011) 28–33.
[33] F. Cardarelli, Materials Handbook – A Concise Desktop Reference, 2nd ed., Springer, London, U. K, 2008.
[34] W. Pabst, E. Gregorová, T. Uhlířová, Microstructure characterization via stereological relations – a shortcut for beginners, Mater. Charact. 105 (2015) 1–12.
[35] M.K. Fahad, Stresses and failure in the diametral compression test, J. Mater. Sci. 31 (2003) 3723–3729.
[36] B.W. Darvel, Review: uniaxial compression tests and the validity of indirect tensile strength, J. Mater. Sci. 25 (1990) 757–780.
[37] J.L. Amorós, V. Cantavella, J.C. Jarque, et al., Green strength testing of stresses compacts: an analysis of the different methods, J. Eur. Ceram. Soc. 28 (2008) 701–710.
[38] N. Ozkan, B.J. Briscoe, Characterization of die-pressed green compacts, J. Eur. Ceram. Soc. 17 (1997) 697–711.
[39] A.T. Procopio, A. Zavaliangos, J.C. Cunningham, Analysis of the diametrical compression test and the applicability to plastically deforming materials, J. Mater. Sci. 38 (2003) 3629–3639.
[40] O.A. Al-Harbi, C. Özgür, M.M. Khan, Fabrication and characterization of single phase cordierite honeycomb monolith with porous wall from natural raw materials as catalyst support, Ceram. Int. 41 (2015) 3526–3532.
[41] S. De Aza, J.E. De los Monteros, Mecanismos de la formación de cordierita en cuerpos cerámicos (Mechanisms of cordierite formation in ceramic bodies), in: Proceedings of the IV Scientific-Technical Conference Glass and Fine Ceramic, Varna, Bulgaria, 1972, pp. 4–7.
[42] J.M. Benito, X. Turrillas, G.J. Cuello, et al., Cordierite synthesis. A time-resolved neutron diffraction study, J. Eur. Ceram. Soc. 32 (2012) 371–379.
[43] R.M. German, Sintering Theory and Practice, 1st ed., John Wiley & Sons, New York, N.Y., 1996.
[44] E. Gregorová, W. Pabst, Process control and optimized preparation of porous alumina ceramics by starch consolidation casting, J. Eur. Ceram. Soc. 31 (2011) 2073–2081.
[45] J.Y. Li, A.I. Yeh, Relationships between thermal, rheological characteristics and swelling power for various starches, J. Food Eng. 50 (2001) 141–148.
[46] Z. Živcová, E. Gregorová, W. Pabst, Low- and high-temperature processes and mechanisms in the preparation of porous ceramics via starch consolidation casting, Starch Staerke 62 (2010) 3–10.
[47] M.H. Talou, M.A. Camerucci, Processing of porous mullite ceramics using novel routes by starch consolidation casting, J. Eur. Ceram. Soc. 35 (2015) 1021–1030.
[48] E. Týnová, W. Pabst, J. Mikač, Starch swelling and its role in modern ceramic shaping technology, Macromol. Symp. 203 (2003) 295–300.
[49] S.J. Gregg, K.S.W. Sing, Adsorption, Surface Area and Porosity, 2nd ed., Academic Press, London, U. K, 1982.
[50] E. Gregorová, Z. Živcová, W. Pabst, Starch as a pore-forming and body-forming agent in ceramic technology, Starch Staerke 61 (2009) 495–502.
[51] M.H. Talou, R. Moreno, M.A. Camerucci, Porous mullite ceramics formed by direct consolidation using native and granular cold-water-soluble starches, J. Am. Ceram. Soc. 97 (2014) 1074–1082.
[52] L.J. Gibson, M.F. Ashby, Cellular solids: Structure and properties, Cambridge Solid State Science Series, 2nd ed., Cambridge University Press, Cambridge, U. K., 1998.
[53] B.H. Mussler, M.W. Shafer, Preparation and properties of mullite-cordierite composites, Ceram. Bull. 5 (1984) 705–714.
[54] G.D. Quinn, J.J. Swab, M.J. Slavin, A proposed standard practice for fractographic analysis of monolithic advanced ceramics, US Army Material technology Laboratory, 1990 (MTL TR 90-57, Technical Report).
[55] G. Carbone, B.N.J. Persson, Crack motion in viscoelastic solids: the role of the flash temperature, Eur. Phys. J. E 17 (2005) 261–281.